energies

MDPI

Article

Modeling and Control Strategy of Wind Energy Conversion System with Grid-Connected Doubly-Fed Induction Generator

Abrar Ahmed Chhipa [1], Prasun Chakrabarti [2], Vadim Bolshev [3,*], Tulika Chakrabarti [4], Gennady Samarin [3,5], Alexey N. Vasilyev [3], Sandeep Ghosh [6] and Alexander Kudryavtsev [3]

1 Techno India NJR Institute of Technology, Udaipur 313003, Rajasthan, India
2 Department of Computer Science Engineering, ITM (SLS) Baroda University, Vadodara 391510, Gujarat, India
3 Federal Scientific Agroengineering Center VIM, 109428 Moscow, Russia
4 Department of Chemistry, Sir Padampat Singhania University, Udaipur 313601, Rajasthan, India
5 Department of Agricultural Power Engineering, Northern Trans-Ural State Agricultural University, 625003 Tyumen, Russia
6 Department of Electrical Engineering, Indian Institute of Technology (BHU), Varanasi 221005, Uttar Pradesh, India
* Correspondence: vadimbolshev@gmail.com; Tel.: +7-499-174-85-95

Abstract: The most prominent and rapidly increasing source of electrical power generation, wind energy conversion systems (WECS), can significantly improve the situation with regard to remote communities' power supply. The main constituting elements of a WECS are a wind turbine, a mechanical transmission system, a doubly-fed induction generator (DFIG), a rotor side converter (RSC), a common DC-link capacitor, and a grid-side converter. Vector control is center for RSC and GSC control techniques. Because of direct and quadrature components, the active and reactive power can also be controller precisely. This study tracks the maximum power point (MPP) using a maximum power point tracking (MPPT) controller strategy. The MPPT technique provides a voltage reference to control the maximum power conversion at the turbine end. The performance and efficiency of the suggested control strategy are validated by WECS simulation under fluctuating wind speed. The MATLAB/Simulink environment using simpower system toolbox is used to simulate the proposed control strategy. The results reveal the effectiveness of the proposed control strategy under fluctuating wind speed and provides good dynamic performance. The total harmonic distortions are also within the IEEE 519 standard's permissible limits which is also an advantage of the proposed control approach.

Keywords: wind energy conversion system; doubly-fed induction generator; MPPT; vector control; renewable energy; WECS; DFIG

Citation: Chhipa, A.A.; Chakrabarti, P.; Bolshev, V.; Chakrabarti, T.; Samarin, G.; Vasilyev, A.N.; Ghosh, S.; Kudryavtsev, A. Modeling and Control Strategy of Wind Energy Conversion System with Grid-Connected Doubly-Fed Induction Generator. *Energies* **2022**, *15*, 6694. https://doi.org/10.3390/en15186694

Academic Editor: King Jet Tseng

Received: 16 August 2022
Accepted: 9 September 2022
Published: 13 September 2022

1. Introduction

Energy has been a remarkable source and a prominent need for the technological evolution of human race. Power generation systems have grown in size in order to meet the increasing electricity demand of the 21st century. Urbanization and expeditious growth in population has engendered a global energy shortage. On the basis of exhaustibility, power generation systems are categorized under two major groups known as renewable energy systems and non-renewable energy systems. Renewable energy is acquired from natural resources such as the sun, biofuel, wind, water stream, geothermal and tides, whereas non-renewable energy is derived from finite sources like nuclear fuels and fossil fuels (coal, crude oil and natural gas) [1].

With the increase in electrical energy demand and reduction of conventional energy sources, it is necessary to increase electrical energy generation through renewable energy sources like wind, solar, etc. [1,2]. Even today, fossil fuels like coal and gas-based electric power generation dominate worldwide, with steam power plants covering a significant

part of per-capita electricity generation. The power systems based on fossil fuels thus form the primary source of energy and seek continuous improvements in different areas such as reliability, stability, controllability, and environmental aspects. Inadequate quality control, aided by high maintenance costs, contributes to the increase in energy bills to the utility and end consumer. Further, fossil fuels such as coal, gas, and petroleum are limited reserves and produce harmful air pollution [3,4]. In addition, nuclear power plants produce harmful radioactive waste, e.g., isotopes of plutonium which cause health hazards to humans and other living bodies including agricultural ones. Also, the maintenance cost of the nuclear power plant is much more than any other power station [5]. Apart from the harmful wastes, environmental issues, high operational costs, and maintenance issues, fossil fuels are limited in quantity and shall vanish one day [6].

Fortunately, nature has provided us alternate energy sources such as wind, solar, geothermal tidal, and fuel cell, which are available abundantly in rural areas and shall be there forever. Wind energy remains a prominent and cleaner energy source among all candidates for naturally available green energy due to its emission-free nature [7].

Wind energy conversion systems (WECS) have become the fastest-growing source of electrical power generation globally and shall cover a significant share of global electricity capacity in the future. Developing countries can quickly adopt this technology owing to its lesser complexity in design, manufacturing, and installation.

The wind turbine converts the kinetic wind power stroked on the rotor blades to mechanical rotational energy. Based on the rotor speed, Wind turbines are categorized as fixed speed wind turbines (FSWT) and variable speed wind turbines (VSWT). The rotational speed is preserved as constant for every wind speed in the FSWT system. The VSWT has the ability to vary their rotor speed to succeed the instantaneous wind speed variations. Generally, the variable-speed turbines are more engrossing than the fixed-speed turbines where the speed of wind varies significantly. There are various reasons for using VSWT over the unreliable operating speed in WECS, these include reduced stress in mechanical parts, reduction in acoustic noise and exalted power quality.

DFIG-based WECS are preferred and are employed worldwide. Such systems consist of a slip ring induction motor or wound rotor induction machine as an electrical power conversion device known as a doubly-fed induction generator [8–10]. They are controlled with electronic converters, making it possible to control the speed of the rotor and power. In the wound rotor induction machine, the stator is directly connected to the grid, and back-to-back connected converters connect rotor windings. It is known as DFIG as it allows the flow of electrical energy in both directions; into the grid when generator operating speed is super-synchronous and into the rotor, if generator speed is sub-synchronous [11]. The bidirectional AC/DC/AC converters, which are connected in between rotor circuit and grid, control the speed above the synchronous speed, and the power is generated from both stator and rotor [12,13].

The main advantages of DFIG are as follow [14,15]:

- Able to supply the power at constant voltage and frequency while the speed of the rotor varies.
- Improve the efficiency of wind generator, rotor speed may vary according to wind speed.
- Power electronic converters require lower power ratings as they have to handle a fraction of the total power.
- Independent control of active and reactive power is possible, and so the power factor can be controlled [16].

The effectiveness of a DFIG-based wind system has been gauged higher than the other wind power generators and so it is an agreeable option for grid-connected wind energy systems driven by VSWT. By considering the favourable features of a DFIG machine, this research work dealt with a DFIG-based VSWT, for wind power applications.

The main power flows out of the stator and is fed to the grid through the generator and transformer. The power handling capacity of the back-to-back converter is about 30%

of the rated power. This back-to-back converter works as a bisectional power flow. The rotor power is first converted to DC by rotor side converter (RSC) [17], then this DC is again converted to AC utilizing grid side converter (GSC) [18] and fed to the grid via the transformer. In wind speed variation, these converters prevent the machine from damage and support the grid line [19]. The RSC is responsible for the active, reactive power exchange to the grid. GSC controls the DC link voltage and grid point of the common coupling power factor utilizing reactive power exchange [20].

Climatic changes and their uncertain nature are major factors that determine the reliability of wind energy. Despite these above-mentioned factors, wind energy system retains some more challenges for researchers, including utility grid integration and the locus of wind turbine. Since the power obtained from the WECS is directly proportional to the wind speed, even a slight variation in wind speed leaves a strong impression in the extracted power. Also, the electrical grid should be extended at constant amplitude and frequency; hence the evoked wind power will be incompatible with the utility grid [21,22].

The unbalanced grid voltage may shrink the span of gearbox and DC-link capacitor owing to plentiful electric torque pulsation. Further, inadequate damped oscillation in the course of voltage sags leads to inferior low-voltage ride through capability. Direct power control, AC grid power fluctuations, direct torque control and decoupled control of the active and reactive power are some additional concerns that are to be considered with regard to WECS [23]. Because of these, some appropriate control schemes have to be employed in order to harvest the maximum power and incur the constant voltage in wind energy applications.

Wind power generation depends on geographical and weather conditions. Thus, developing such advanced types of control strategies can make the system work with maximum efficiency and produce optimum power considering grid codes and IEEE standards [24]. Our study focuses on vector control based on the voltage and flux vector in *dq* reference frame, which provides independent control of active and reactive power.

This paper is organized as follows: Section 1 discusses the importance of the use of DFIG-based WECS. Section 2 presents a literature survey in terms of technology development in the field of wind energy conversion system. In Section 3 we present the system configuration of grid-connected DFIG-based WECS and the modeling of wind turbine and doubly-fed induction generators. Section 4 describes the MPPT controller for optimum torque reference generation in RCS. Section 5 presents the vector control strategy for RCS and GCS, which are based on PI controller. At last, in Sections 6 and 7, we conclude the study by a simulation analysis and simulation results of the proposed system control with variable input wind speed.

2. Literature Survey

This section deals with the literature survey in terms of state of the art and significant developments in the area of wind energy conversion systems. It is based on its classification into two broad categories: fixed speed wind turbine- and variable speed wind turbine-based generating systems. The literature review on the use of a battery energy storage system with wind energy conversion systems is also carried out in detail. In the past, the most commonly used generators were the squirrel cage induction generator (SCIG) in terms of wind turbine generators (WTGs) using fixed speed wind turbines. The use of an isolated asynchronous generator (IAG) for the stand-alone power generation has been proven promising for the last few decades due to its simplicity, brushless construction, ease in maintenance, inherent short circuit protection and large torque/weight ratio [25,26]. Another attempt has been made by Quazene and McPherson [27] to analyze the operation of an IAG in stand-alone WECS. They used an IAG feeding with resistive loads where frequency and voltage were not regulated across the loads. The main barriers in IAG commercial adoption are its poor voltage and frequency regulation characteristics. Further, when the load is directly connected across the IAG bus, the IAG frequency depends on the prime-mover speed which is a function of input wind power and connected consumer

loads [28]. Casielles et al. [28] have reported a control system for a wind turbine driven IAG. In these works, the authors used discrete switching for the number of switched capacitors and resistors to balance active and reactive powers as the wind speed changes. However, the discrete switching of capacitors and resistors has provided an inferior performance of the controller as far as power quality, proficiency and maintenance. It has been shown that a voltage source converter (VSC) facilitates the achievement of better system behavior in terms of voltage regulation, reactive power compensation and frequency stabilization. Kasal and Singh [29] have reported different system configurations of voltage and frequency controllers for an IAG and their design for stand-alone WECS. They compared a DFIG-based, grid-fed WECS with other WECS technologies such as fixed speed and a sensor-less vector control techniques for a DFIG-based stand-alone power generation utilizing model reference adaptive system (MRAS) observer. The sensor-less plan has been approved under both steady-state and transient conditions utilizing exploratory outcomes. Pena et al. [30] have discovered a control scheme for the stand-alone operation of a DFIG supplying inequivalence load. The front-end converter was controlled to compensate for inequivalence loads by supplying positive and negative distributed load currents. Jain and Ranganathan [31] discussed a vector-controlled scheme for back-to-back connected VSC's for a DFIG-based stand-alone power generation. In this sensorless control scheme, the function of active filtering was introduced for a DFIG based stand-alone energy conversion system. Harmonics present in the consumer loads were compensated through a front-end converter. Goel et al. [32] announced that two DFIGs connected parallelly worked for stand-alone WECS feeding nearby loads. In this control, the authors utilized three VSC's for the control of two parallel operated DFIG's. The BESS was utilized in the middle of the DC-link of three VSC's for load levelling. Variable speed wind turbines are presently utilized as a part of WECS innovation. The variable speed activity is possible because the power that the electronics converters provide allows for complete decoupling from the grid. Full rating variable-speed WECS are flexible in terms of different types of generators used in these WECSs. Watson et al. [33] proposed an IAG-based variable speed WECS for controllable DC control supply. A three-phase controlled rectifier was utilized at the generator side to change variable voltage/variable frequency AC supply to a constant supply DC voltage. The reactive power demand of an IAG was met by using the self-excitation capacitors and the proper controls variable speed IAG-based WECS technologies was done. It has been proven through the obtained results that a DFIG-based WECS has been suggested due to its enhancement of the wind energy capturing capacity for the same rating of another machine in WECS [34]. The DFIG is the only machine that can give more than its rated power without being overloaded [35,36]. The DFIG has the capability to produce power under the change in prime-mover speed at constant voltage and frequency. Further, the DFIG can be controlled from the rotor side and it reduces the overall controller rating (i.e., the fraction of the DFIG rating) [37]. These features make a DFIG one of the most attractive choices for variable speed prime-movers. Yamamoto and Motoyoshi [36] have reported that the DFIG-based energy conversion system controls the active and reactive power of the system through back-to-back connected VSC's feeding the generated power to the grid. The literature of different control strategies of a DFIG feeding generating power to the grid is also addressed [37–45]. Some literature is also available on the sensorless operation of a DFIG supplying generating power to the grid [46–48]. In [49], the authors reported an implementation of a vector-controlled DFIG based stand-alone WECS. The execution of the voltage and frequency controller has been shown with linear loads. Cardenas et al. [50] examined how over-firing angles and electrical loads at a DC bus have been proposed for constant DC bus voltage. In [51], authors reported a rule-based fuzzy logic controller for a variable speed IAG-based stand-alone wind energy conversion system. Simoes et al. [52] described the control strategy, design and performance evaluation of a fuzzy logic-based variable speed wind energy conversion using an IAG. Poddar et al. [53] reported a variable speed controller for a 225 kW IAG based grid integrated wind energy conversion system using a sensorless control algorithm that was realized using a direct torque control method.

This control algorithm was based on active and reactive power control. In [54] the authors suggest proposing an automatic mode switch control strategy for IAG-based small wind turbines under conditions of grid failure in the stand-alone mode of a grid-connected system. In [55,56] the authors describe a phase-locked loop (PLL) control configuration for a vector-controlled capacitor-excited IAG that uses PWM controlled VSC converters for AC and DC voltage regulation in variable speed WECS. Barakati et al. [57] propose a grid converter for an IAG-based variable speed WECS integrated with the grid. In this work, the authors propose a single-stage conversion in place of two-stage conversion with AC-DC-AC converters. The effectiveness of the controller has been shown through simulation results. Agrawal et al. [58] have reported a novel maximum power tracking algorithm using a grid converter for an IAG-based WECS. Vas and Li [59] have developed a package for simulating the performance of a vector-controlled generator and named it SIMUVEC, applicable for both voltage source and current source inverter fed induction motors. Gabriel et al. [60] have presented a field-oriented control of AC motors using microprocessors. The change of the transient stability margin of the network wi th increment in wind power penetration when the wind farms are associated with the distinguished areas, whereas the stability condition deteriorates with increased penetration when the DFIG is connected to with some other location. Yuan-Kang Wu et al. [61] presented different control strategies in the rotor side converter of a 2 MW DFIG wind turbine. these control strategies are operated on MPPT mode to obtain maximum efficiency. These are categories such as voltage-oriented control, flux oriented control, direct torque control and direct power control. The performance was obtained under these strategies and simulated by PSCAD/EMTDC software[61].

3. System Configuration and Modeling of DFIG

The system configuration of a grid-connected DFIG-based WECS is shown in Figure 1. This configuration is designed to deliver the power of 2 MW. The system comprises a wind turbine, DFIG, rotor-side filter, grid side filter, MPPT controller, DC-link capacitor, and back-to-back three-phase pulse width modulated (PWM) VSCs with their controller. The VSC connected to the rotor winding through the rotor filter is named RSC. The stator winding is directly connected to the grid, and the VSC is connected at the point of coupling (PoC) in GSC [62]. The RSC and GSC are responsible for achieving the different operating conditions of DFIG. The block scheme of the proposed system is shown in Figure 2.

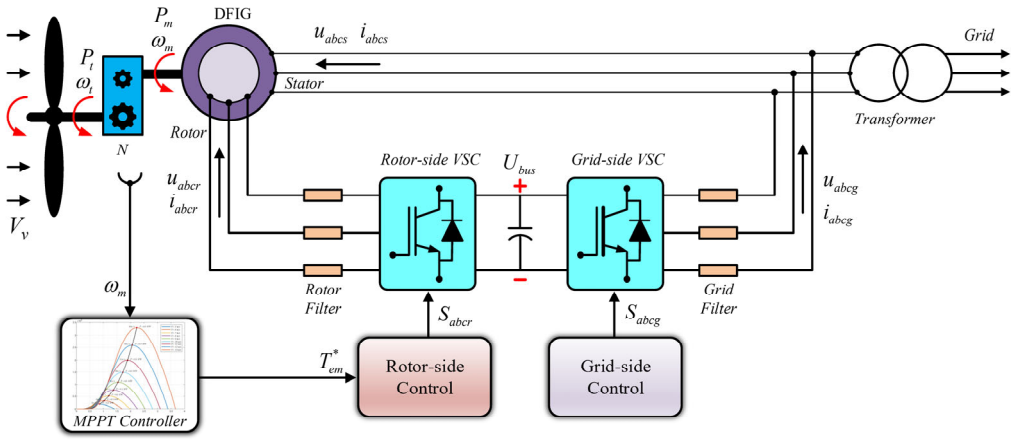

Figure 1. Configuration of variable speed wind turbine with DFIG.

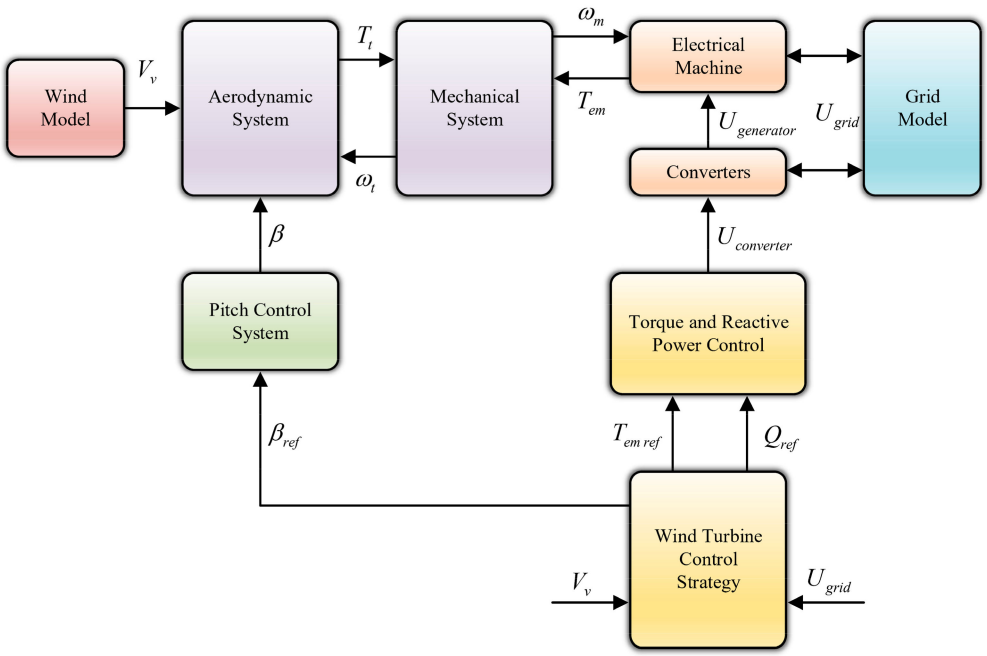

Figure 2. Block diagram of a grid-connected DFIG.

3.1. Wind Turbine Modeling

The kinetic energy of the wind is converted to rotational energy in the form of a torque by the wind turbine (WT). The power available in the wind is given by Equation (1):

$$P_v = \frac{1}{2}\rho A V_v^3 \tag{1}$$

where

A: Area swept by turbine blades (m^2).
ρ: The air density (kg/m^3).
V_v: Wind speed (m/s).

The power extracted by the turbine from the available power in the wind is given by Equation (2):

$$P_t = \frac{1}{2}\rho\pi R^2 V_v^3 C_p(\lambda,\beta) \tag{2}$$

where

R: The radius of turbine rotor (m)
$C_p(\lambda,\beta)$: The power coefficient
C_p is a function of tip speed ratio (λ) and the pitch angle (β).

$C_p(\lambda,\beta)$ is expressed by Equation (3) and Equation (4):

$$C_p(\lambda,\beta) = c_1\left(\frac{c_2}{\lambda_i} - c_3\beta - c_4\beta^{c_5} - c_6\right).e^{\frac{-c_7}{\lambda_i}} \tag{3}$$

where $c_1 = 0.73;\ c_2 = 151;\ c_3 = 0.58;\ c_4 = 0.002;\ c_5 = 2.4;\ c_6 = 13.2;\ c_7 = 18.4$

$$C_p(\lambda,\beta) = 0.73.\left(\frac{151}{\lambda_i} - 0.58\beta - 0.002\beta^{2.4} - 13.2\right).e^{\frac{-18.4}{\lambda_i}} \tag{4}$$

$$\lambda_i = \frac{1}{\lambda + 0.02\beta} - \frac{0.003}{\beta^3 + 1} \tag{5}$$

According to the Betz limit, the maximum theoretical value C_p is expressed in Equation (6):

$$C_{p\ Theo\ \max} = 0.593 = 59.3\% \tag{6}$$

The λ is expressed in Equation (7):

$$\lambda = \frac{R\omega_t}{V_v} \tag{7}$$

The turbine generated torque is expressed in Equation (8):

$$T_t = \frac{P_t}{\omega_t} \tag{8}$$

ω_t: The angular rotational speed of wind turbine rotor (rad/sec).

3.2. DFIG Modeling

The DFIG is composed of stator and rotor windings. It features slip rings. Three-phase insulated windings are mounted on the stator connected to the grid through a three-phase transformer. The rotor is also built of three-phase insulated windings in the same way as the stator. A set of slip rings and brushes connects the rotor windings to an external stationary circuit. These components allow for either injection into or absorption from the rotor windings of the control rotor current [62–65].

The direct and inverse transformation is used to represent the dynamic model of the DFIG. Using space vector theory, the three windings of the rotor and stator can be represented by two winding $\alpha\beta$ as stationary for stator and winding dq as rotating for the rotor.

The stator and rotor voltage vector is expressed as:

$$\vec{u}_s \Rightarrow \begin{cases} u_{ds} = R_s i_{ds} + \frac{d\psi_{ds}}{dt} - \omega_s \psi_{qs} \\ u_{qs} = R_s i_{qs} + \frac{d\psi_{qs}}{dt} + \omega_s \psi_{ds} \end{cases} \tag{9}$$

$$\vec{u}_s \Rightarrow \begin{cases} u_{dr} = R_r i_{dr} + \frac{d\psi_{dr}}{dt} - \omega_r \psi_{qr} \\ u_{qr} = R_r i_{qr} + \frac{d\psi_{qr}}{dt} + \omega_r \psi_{dr} \end{cases} \tag{10}$$

where u_{ds}, u_{qs}, u_{dr}, and u_{qr}: stator and rotor voltages in the dq frame, respectively. i_{ds}, i_{qs}, i_{dr}, and i_{qr}: stator and rotor current in the dq frame, respectively.R_r, R_s, ω_s and ω_r: stator and rotor phase resistances and angular velocity, respectively. From Equations (9) and (10), dq equivalent electric circuit is represented by Figure 3.

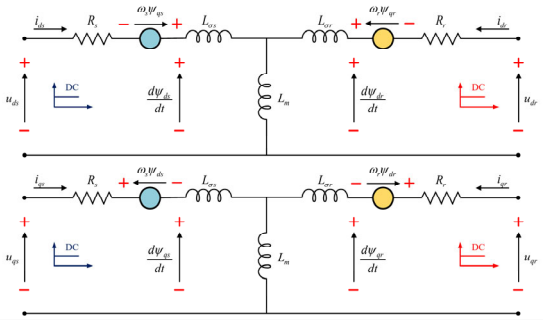

Figure 3. DFIG dq equivalent circuit.

The stator and rotor flux vector are expressed in Equation (11) and Equation (12), respectively:

$$\vec{\psi}_s \Rightarrow \begin{cases} \psi_{ds} = L_s i_{ds} + L_m i_{dr} \\ \psi_{qs} = L_s i_{qs} + L_m i_{qr} \end{cases} \tag{11}$$

$$\vec{\psi}_r \Rightarrow \begin{cases} \psi_{dr} = L_m i_{ds} + L_r i_{dr} \\ \psi_{qr} = L_m i_{qs} + L_r i_{qr} \end{cases} \tag{12}$$

where $\vec{\psi}_s$, $\vec{\psi}_r$ are the flux vectors for stator and rotor, respectively. ψ_{ds}, ψ_{qs} are the fluxes along the dq axis stator. ψ_{dr}, ψ_{qr} are the fluxes along with the dq axis rotor. L_s, L_r: stator and rotor phase leakage inductances, respectively, L_m: stator–rotor mutual inductance, and p: is the number of pole pairs of the generator.

The expression of electromagnetic torque is expressed in Equation (13):

$$T_{em} = \frac{3}{2} p \frac{L_m}{L_s} \left(\psi_{qs} i_{dr} - \psi_{ds} i_{qr} \right) \tag{13}$$

The active and reactive power equations of the stator and rotor are given by Equation (14) and Equation (15):

$$\begin{cases} P_S = \frac{3}{2} \left(u_{ds} i_{ds} + u_{qs} i_{qs} \right) \\ Q_S = \frac{3}{2} \left(u_{qs} i_{ds} - u_{ds} i_{qs} \right) \end{cases} \tag{14}$$

$$\begin{cases} P_r = \frac{3}{2} \left(u_{dr} i_{dr} + u_{qr} i_{qr} \right) \\ Q_r = \frac{3}{2} \left(u_{qr} i_{dr} - u_{dr} i_{qr} \right) \end{cases} \tag{15}$$

where P_s, Q_s present stator active and reactive power, respectively. P_r, Q_r presents rotor active and reactive power, respectively. T_{em} is the electromagnetic torque.

The fundamental torque expression is expressed by Equation (16):

$$T_{em} - T_{load} = J \frac{d\omega_m}{dt} \tag{16}$$

With J representing the inertia of the rotor, T_{load} the load torque applied to the shaft and ω_m the rotor speed.

4. MPPT Control

WT consist of four control regions, the wind turbine speed as a function of wind speed is shown in Figure 4. These operating zones can be expresses as follows:

- Zone-1: In this region, speed is very low as the WT cannot generate the power.
- Zone-2: This control zone tracks the restoration of maximum power limited by minimum wind speed to the rated value.
- Zone-3: In this region, the WT operates with rated maximum speed. However, power output is not maximum.
- Zone-4: In this zone, the WT generates maximum rated power. Beyond maximum allowable wind speed, protection devices get activated to avoid failure or damage of WT.

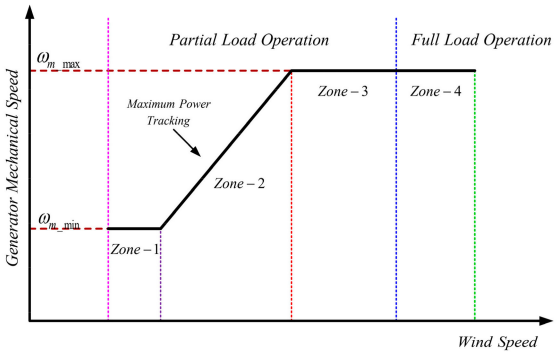

Figure 4. WT control regions.

The main objective of the MPPT controller is to deliver optimal power by DFIG WECS. Here MPPT is used to control the RSC by selecting optimum torque reference for the

generator. C_p must be maintained to its $C_{p\,\max}$ value to reach the optimum value of torque given by the Equation (18). Figure 5 illustrate the control region range.

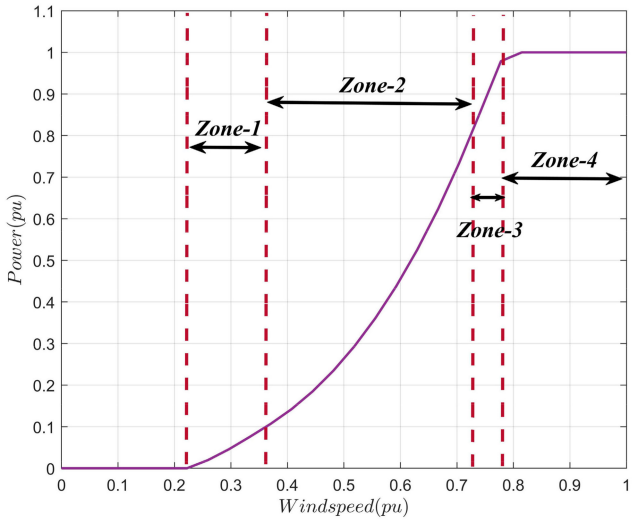

Figure 5. Control region range.

In several studies, different methods have been proposed for wind turbine power extraction [66]. When the WT operate on MPPT, expressions are given by Equation (17):

$$\begin{cases} \lambda_{opt} = \frac{R\omega_t}{V_v} \\ C_p = C_{p\max} \end{cases} \tag{17}$$

The torque is expressed by Equation (18):

$$T_t = \frac{1}{2}\rho\pi\frac{R^5}{\lambda_{opt}^3}C_{p\max}\omega_t^2 = K_{opt}\omega_t^2 \tag{18}$$

where

$$K_{opt} = \frac{1}{2}\rho\pi\frac{R^5}{\lambda_{opt}^3}C_{p\max},\ \beta_{opt} = 0^\circ,\ \omega_m = N\omega_t$$

ω_t is the speed of rotation of the turbine, ω_m is the mechanical speed and N is the multiplier coefficient. Proposed MPPT is presented in Figure 6.

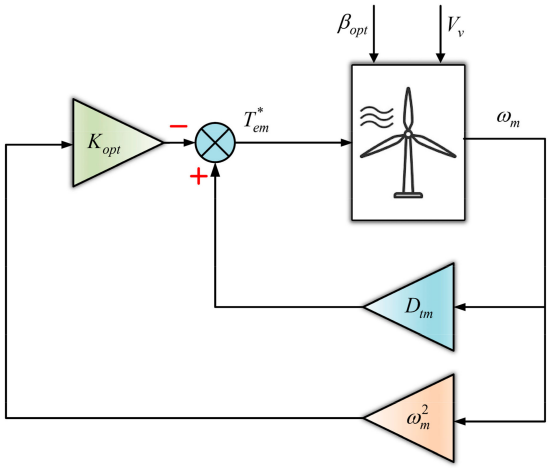

Figure 6. Indirect speed MPPT control.

5. Control Strategy for RSC and GSC

The three-phase grid voltage supplies the DFIG stator winding at constant magnitude and frequency. In contrast, the rotor is supplied at different magnitudes and frequencies by RSC to attain different operating conditions of DFIG. The operating point of the machine decides the power flow through the rotor and grid. The three operating modes of DFIG depend on the speed given in Equation (20):

$$\begin{cases} \omega_s = \omega_r + \omega_m \\ s = \frac{\omega_s - \omega_m}{\omega_s} \end{cases} \tag{19}$$

$$\begin{cases} \omega_m < \omega_s \Rightarrow \omega_s > 0 \Rightarrow s > 0 \Rightarrow Subsynchronous\ operation \\ \omega_m > \omega_s \Rightarrow \omega_r < 0 \Rightarrow s < 0 \Rightarrow Hypersynchronous\ operation \\ \omega_m = \omega_s \Rightarrow \omega_r = 0 \Rightarrow s = 0 \Rightarrow Synchronous\ operation \end{cases} \tag{20}$$

In vector control, a strategy is utilized in *dq* frame with DFIG. This naturally decouples the *d* and *q* quantities. Decoupling makes the DFIG operate as a DC motor. The stator flux vector is aligned along the d axis, as shown in Figure 7.

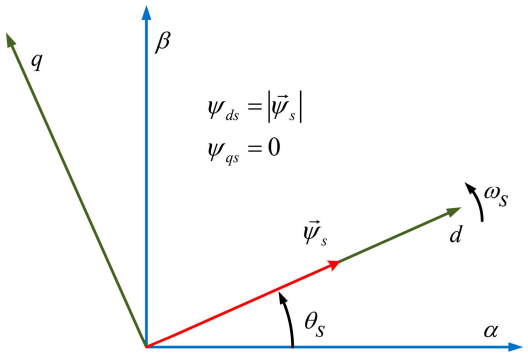

Figure 7. The stator flux vector aligned with d axis component.

5.1. Rotor Side Control

The RSC applies the voltage at rotor winding. Substituting Equations (11) and (12) into Equation (10) gives voltage equations in *dq* frame, considering $\psi_{qs} = 0$ yields the following voltage expressions:

$$\begin{cases} u_{dr} = R_r i_{dr} + \sigma L_r \frac{di_{dr}}{dt} - \omega_r \sigma L_r i_{qr} + \frac{L_m}{L_s} \frac{d\vec{\psi}_s}{dt} \\ u_{qr} = R_r i_{qr} + \sigma L_r \frac{di_{qr}}{dt} + \omega_r \sigma L_r i_{dr} + \omega_r \frac{L_m}{L_s} \frac{d\vec{\psi}_s}{dt} \end{cases} \tag{21}$$

where $\sigma = 1 - L_m^2 / L_s L_r$. Due to the fixed grid quantities $d\vec{\psi}_s / dt$ near to zero, the stator winding resistance drop can be neglected, and the stator flux can be treated as constant. It is evident from Equation (21) that the regulators can be employed to control the *dq* component of rotor current. REG-1 represents the reactive power proportional–integral (PI) regulator. For both *d* and *q* current loops, equal PI regulators are chosen and presented as REG-2 and REG-3, respectively. The gain parameter of the regulator is tuned by considering actual values only. Table 1 represents the value for gain parameters for all three of the regulators. In order to transform the rotor voltage and current into *dq* components using *abc–dq* transform, it is compulsory to apply the control strategy on the *dq* components. Θ_s is obtained by first estimating the stator voltage vector and subtracting angle $\pi/2$. Grid synchronization is achieved by the phase-locked loop (PLL), which in turn will mitigate minor disturbances. The "u", that is 1/3, defines the turn ratio for stator-rotor.

Table 1. The rotor-side control gain parameter of REG-1, REG-2 and REG-3.

Gains	REG-1	REG-2	REG-3
Proportional	10,160	0.5771	0.5771
Integral	406,400	491.5995	491.5995

Expressions for torque in dq frame may be found in Equation (22):

$$T_{em} = \frac{3}{2} p \frac{L_m}{L_s} \left(\psi_{qs} i_{dr} - \psi_{ds} i_{qr} \right) = \frac{3}{2} p \frac{L_m}{L_s} \psi_{ds} i_{qr} \Rightarrow T_{em} = K_t i_{qr} \tag{22}$$

The equations for stator reactive power in dq frame may be found in Equation (23):

$$Q_s = \frac{3}{2} \left(u_{qs} i_{ds} - u_{ds} i_{qs} \right) = -\frac{3}{2} \omega_s \frac{L_m}{L_s} \vec{\psi}_s \left(i_{dr} - \frac{\vec{\psi}_s}{L_m} \right) \Rightarrow Q_s = K_q \left(i_{dr} - \frac{\vec{\psi}_s}{L_m} \right) \tag{23}$$

Equation (22) reveal that the i_{qr} is proportional to the T_{em}, so torque can be controlled with i_{qr}. Expression in Equation (23) reveals that the Q_s is controlled using the i_{dr}. The RSC control strategy block diagram is presented in Figure 8, which reveals all control loops and MPPT.

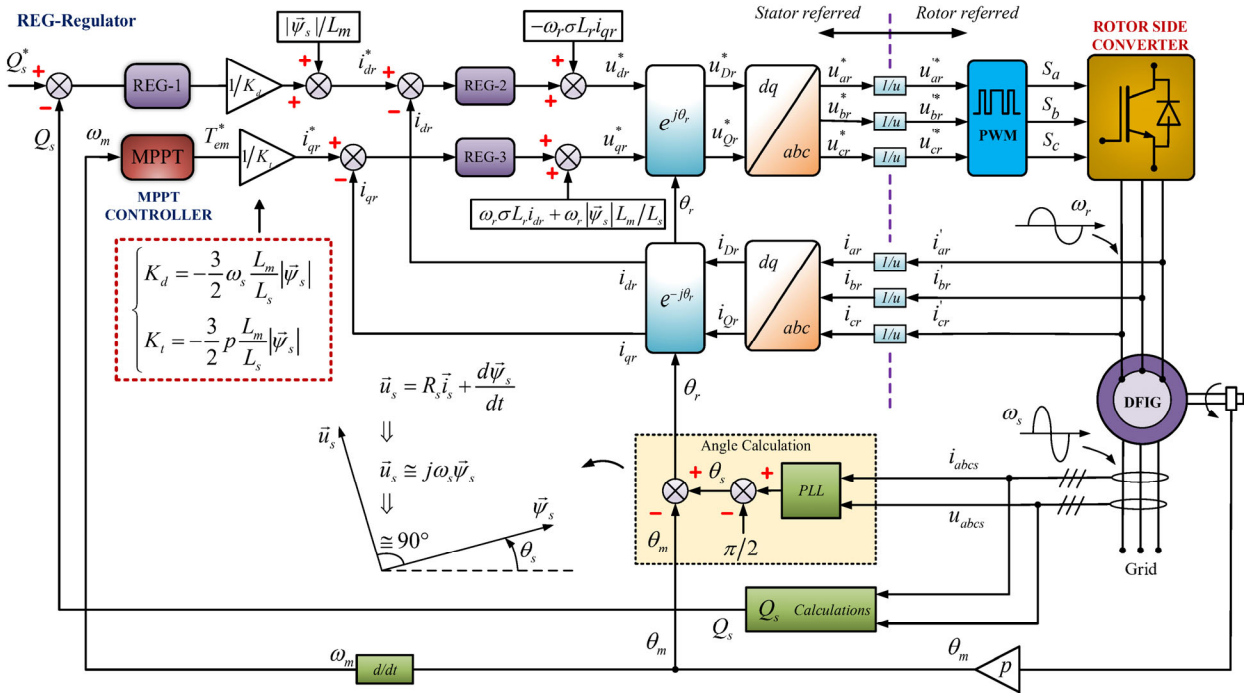

Figure 8. RSC control strategy of the DFIG.

5.2. Grid Side Control

The system configured by the GSC, filter, and grid voltage can be represented as shown in Figure 9. GSC control strategy is used to control the power flow of the DFIG.

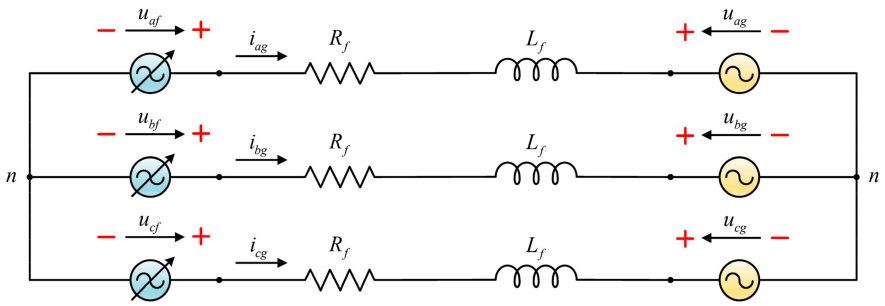

Figure 9. Simplified representation of the three-phase grid system.

Two critical components to consider when controlling the power flow are DC link voltage V_{bus} and reactive power Q_g exchange with grid

Figure 10 presents the dq model of the grid side system in a stationary frame. Figure 11 shows the direct component of voltage vector oriented along the ω_s, considering Equation (24). The dq component of the filter voltage can be expressed by Equation (25) and the expression of the grid exchange active and reactive power in Equation (26).

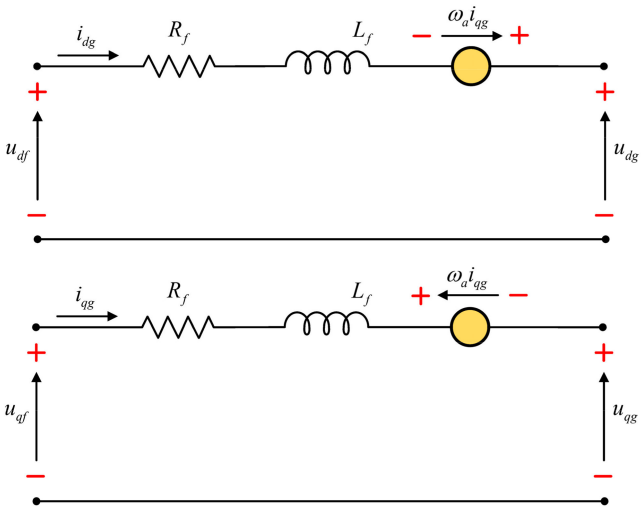

Figure 10. The schematic representation of dq model of the grid side system in the stationary frame.

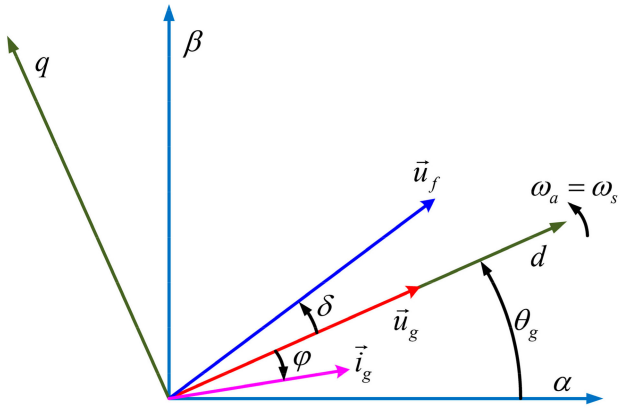

Figure 11. Grid voltage vector oriented along with ω_s.

$$\begin{cases} u_{dg} = \left|\vec{u}_g\right| \\ u_{qg} = 0 \\ \omega_a = \omega_s \\ \theta = \omega_a t \Rightarrow \theta = \theta_g = \omega_s t \end{cases} \tag{24}$$

$$\begin{cases} u_{df} = R_f i_{dg} + L_f \frac{di_{dg}}{dt} + u_{dg} - \omega_s L_f i_{qg} \\ u_{qf} = R_f i_{qg} + L_f \frac{di_{qg}}{dt} + \omega_s L_f i_{dg} \end{cases} \tag{25}$$

$$\begin{cases} P_g = \frac{3}{2}\left(u_{dg} i_{dg} + u_{qg} i_{qg}\right) \Rightarrow P_g = \frac{3}{2} u_{dg} i_{dg} \\ Q_g = \frac{3}{2}\left(u_{qg} i_{dg} - u_{dg} i_{qg}\right) \Rightarrow Q_g = -\frac{3}{2} u_{dg} i_{qg} \end{cases} \tag{26}$$

Equation (26) reveals that the i_{dg} current component controls the P_g, while the i_{qg} current component controls the Q_g value. Figure 12 shows the block diagram of GSC control. A capacitor forms the DC link; active power flows through RSC-Capacitor-GSC to the grid. Therefore, maintaining V_{bus} to a constant value will ensure both RSC and GSC work properly during active power flow. In the same manner, reactive power flow in the grid is ensured. From reference V_{bus} and Q_g, this generates pulses for the GSC switches S_{ag}, S_{bg} and S_{cg}. Vector control strategy for the GSC is shown in Figure 13. The gain parameters for all three regulators in grid-side control are presented in Table 2.

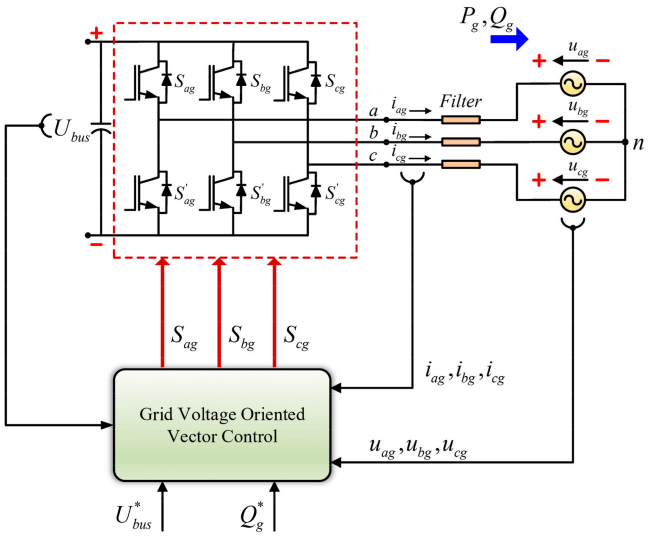

Figure 12. Block diagram of grid-side system.

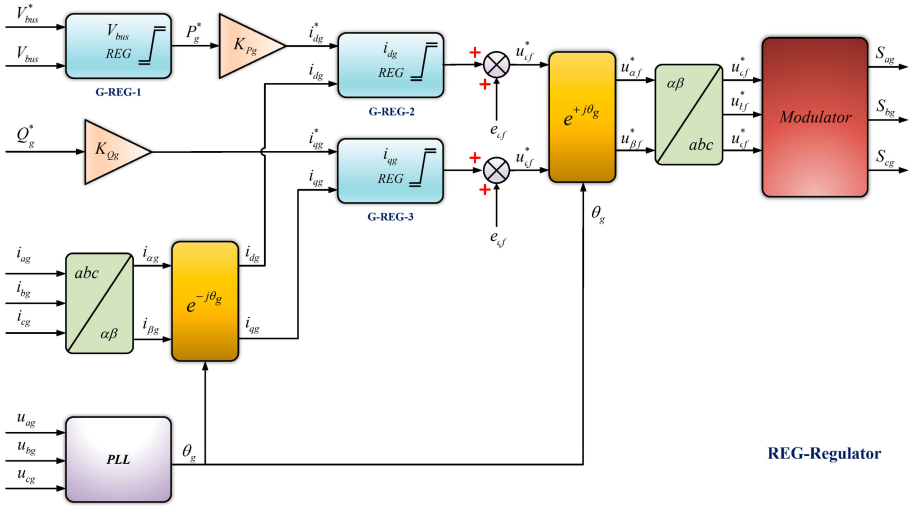

Figure 13. Block diagram of GSC vector control strategy.

Table 2. The gain parameters of PI regulators in grid-side control.

Gains	G-REG-1	G-REG-2	G-REG-3
Proportional	1000	0.3016	0.3016
Integral	300,000	56.8489	56.8489

For improved performance and dynamic response, the coupling term at each current controller output is added by Equation (27). The constant term K_{Pg} and K_{Qg} can be derived from Equation (26) presented in Equation (28).

$$\begin{cases} e_{df} = -\omega_s L_f i_{qg} \\ e_{qf} = \omega_s L_f i_{dg} \end{cases} \tag{27}$$

$$\begin{cases} K_{Pg} = \frac{1}{\frac{3}{2}u_{dg}} \\ K_{Pg} = \frac{1}{-\frac{3}{2}u_{dg}} \end{cases} \tag{28}$$

6. Simulation Results

The proposed DFIG modeling and control of RSC and GCS are implemented and simulated in MATLAB/Simulink environments. In this section, the performance of the proposed system is analyzed during wind speed variation. The simulation parameters of the system are presented in Table 3.

Table 3. Model Simulation Parameters.

Parameter	Parameter Value	Parameter	Parameter Value
Nominal wind speed	11 m/s	Frequency	50 Hz
Air density	1.225 kg/m^3	Rated torque	12,732 N·m
Tip speed ratio	7	Pole pair	2
Pitch angle	0°	Inertia	127 kg·m^2
Power coefficient	0.4411	Gear ratio	100
Nominal Power	2 MW	Radius of turbine	42 m

In this work, β is set to zero and designed for the rated wind speed of 11 m/s. The simulated power characteristics at $\beta = 0^{\circ}$ and different wind speed is presented in Figure 3.$C_p - \lambda_i$ characteristics at different value of β is presented in Figure 14. The design shows that the maximum value of $C_{p\,\max}$ is 0.4411 and corresponding λ is 7 at $\beta = 0^{\circ}$ is

shown in Figure 15. This value of $C_{p\,\max}$ and λ is optimum value for capturing peak power from the available wind power.

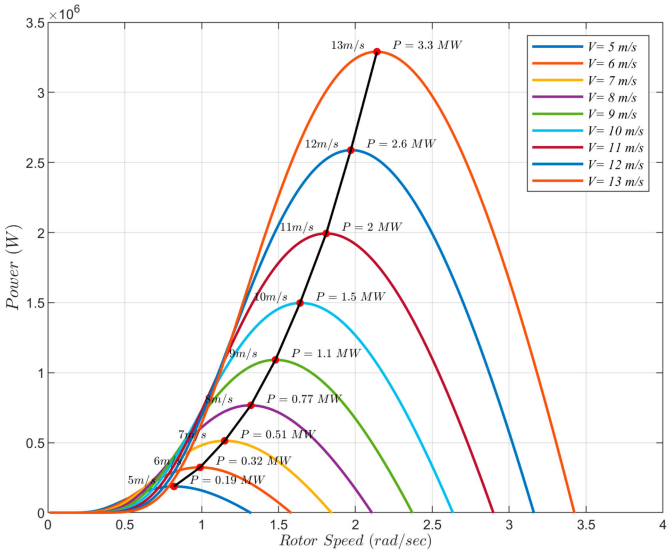

Figure 14. Power and rotor speed characteristics of WT at different wind speed.

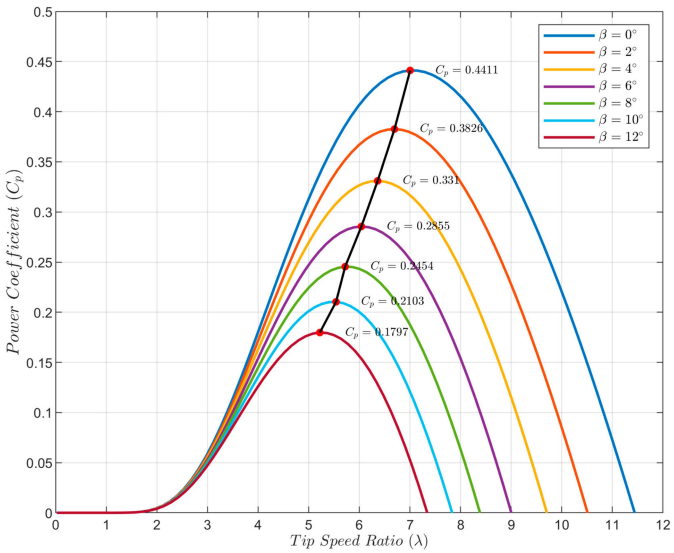

Figure 15. Characteristics with variation in pitch angle (β).

Figure 16 represents the model of DFIG in MATLAB/Simulink environment. Figures 17 and 18 show the Simulink modeling of the RSC control and GSC control.

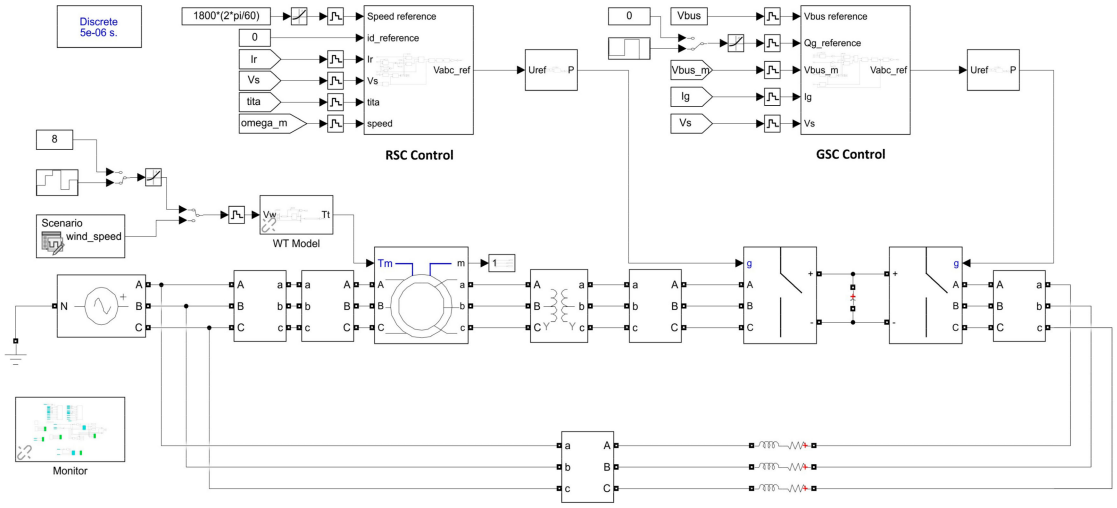

Figure 16. Simulink model of grid-connected DFIG.

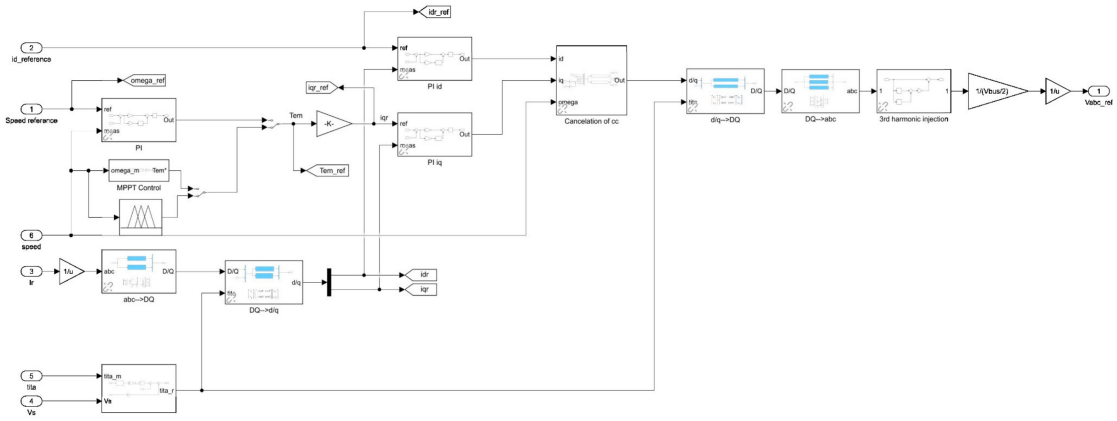

Figure 17. Rotor side control block.

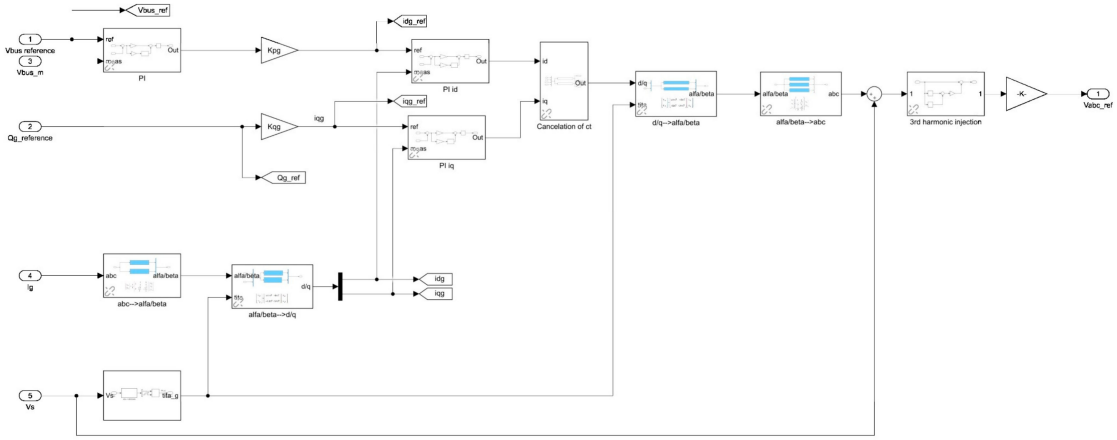

Figure 18. Grid side control block.

The wind speed profile applied to the system is depicted in Figure 19. The wind speed profile has a wide speed range variation between 7 to 12 m/s. In this simulation study the ramp increase and ramp decrease of wind speed is considered. At the start of the simulation a wind speed of 7 m/s is considered, and the system starts simulating from stand steel condition. Figure 20 presents the simulation response of theoretical and actual

rotor speed tracking related to the wind speed variation. It can be seen that the proposed control scheme performs well in terms of the tracking of speed.

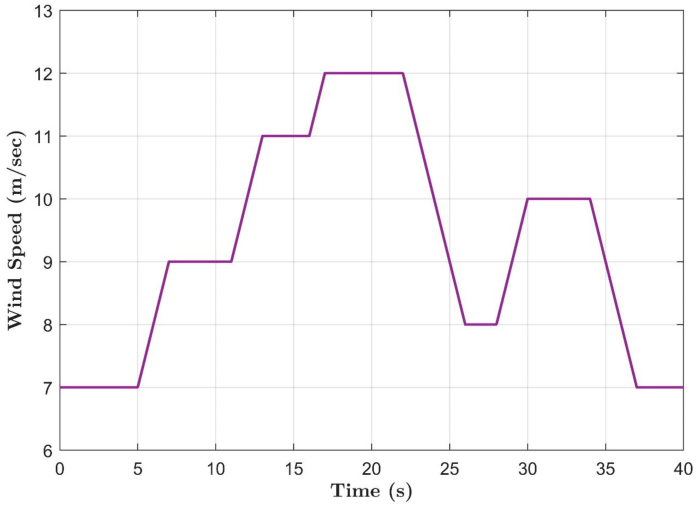

Figure 19. Wind speed variation input to the system.

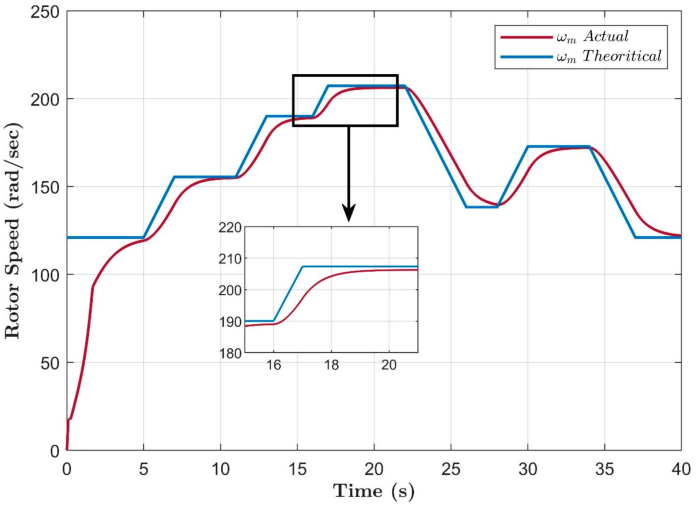

Figure 20. Response of actual and theoretical rotor speed.

Figure 21 shows the variation in the power coefficient (C_p) and tip speed ratio (λ). The blue line represents the C_p and the orange line represents the λ. According to the Betz limit, the maximum theoretical value C_p is expressed in Equation (6) and the optimal value for the proposed system is 0.4411 at zero pitch angle as represented in Figure 15. During the complete simulation, the proposed controllers keep this near to this optimal value which shows a minimal variation C_p between 0.42 to 0.45 due to the excellent perturbation of the MPPT controller. The tracking performance of the electromagnetic torque is presented in Figure 22, which shows the torque reference produced by the MPPT controller and the actual torque of DFIG.

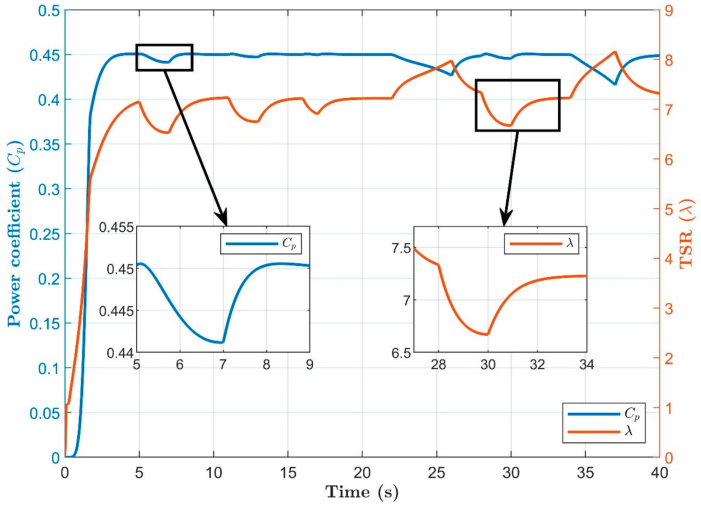

Figure 21. Response of power coefficient and tip speed ratio variation.

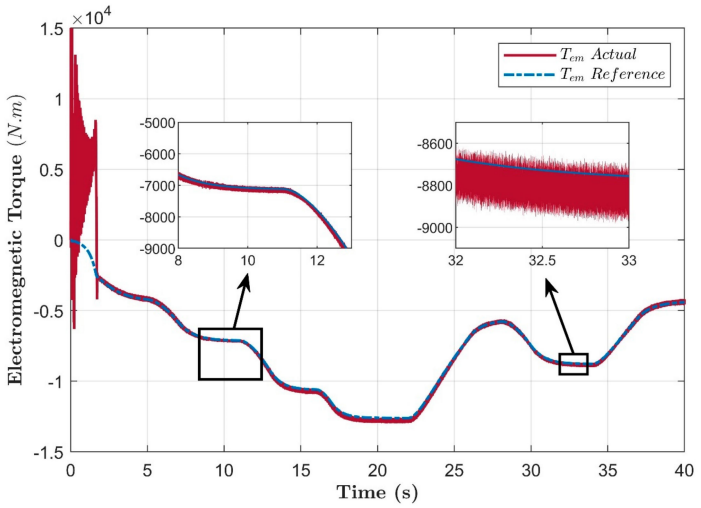

Figure 22. Reference and actual electromagnetic torque tracking.

The stator current and rotor current response during the simulation is presented in Figures 23 and 24, respectively. Figure 25 shows that the single-phase stator voltage and current are balanced and sinusoidal according to the IEEE 519 standard.

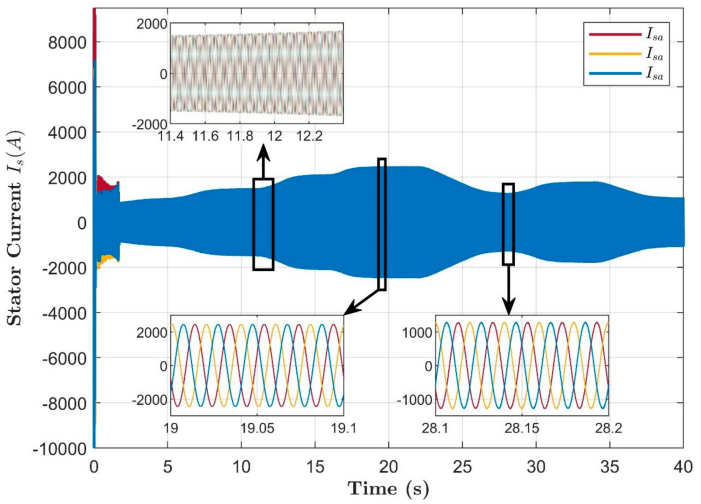

Figure 23. DFIG stator current variation.

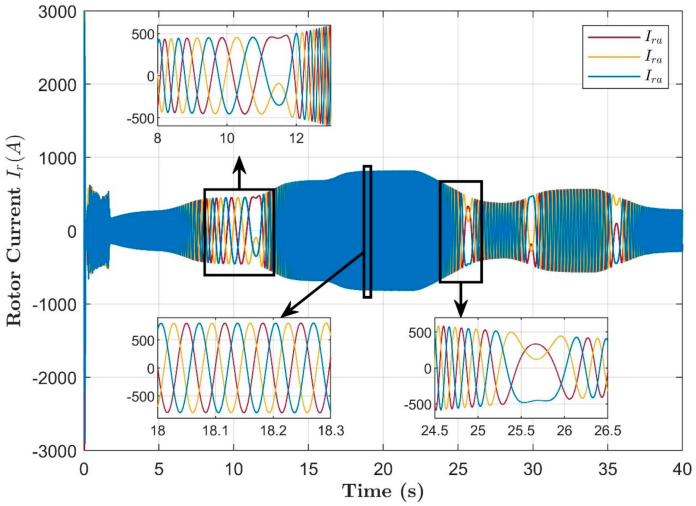

Figure 24. DFIG rotor current variation.

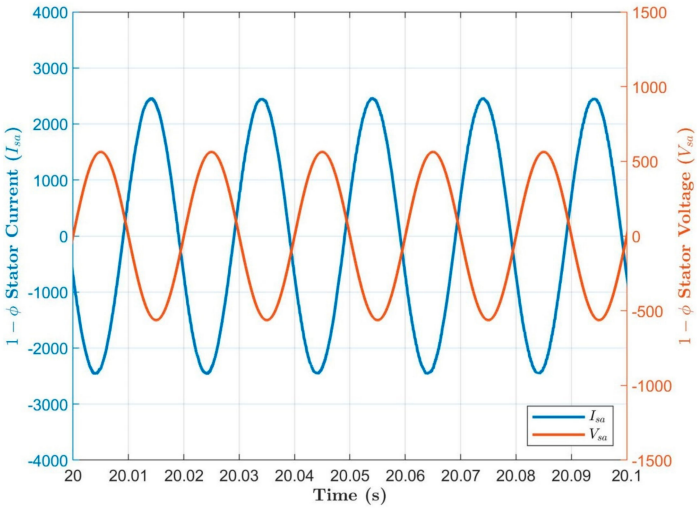

Figure 25. Single phase voltage and current of DFIG stator.

Figure 26 presents the stator active power performance according to wind speed variation. MPPT controller shows excellent dynamic performance during the wind speed variation. As seen in Figure 26, power output at a wind speed of 12 m/s is 1.978 MW. Grid side reactive power tracking performance according to reactive reference power is shown in Figure 27. At t = 10 s, reactive power reference is changed from 0 to -4×10^5, the controller performance shows that the reactive power follows the reference without significant overshoot.

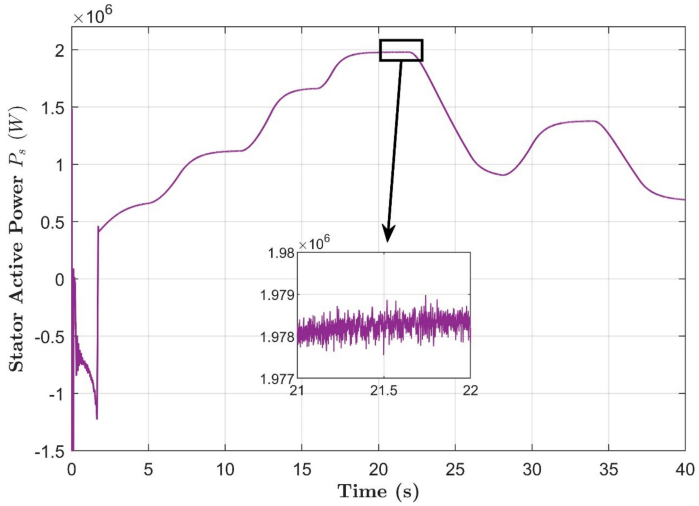

Figure 26. Stator active power variation.

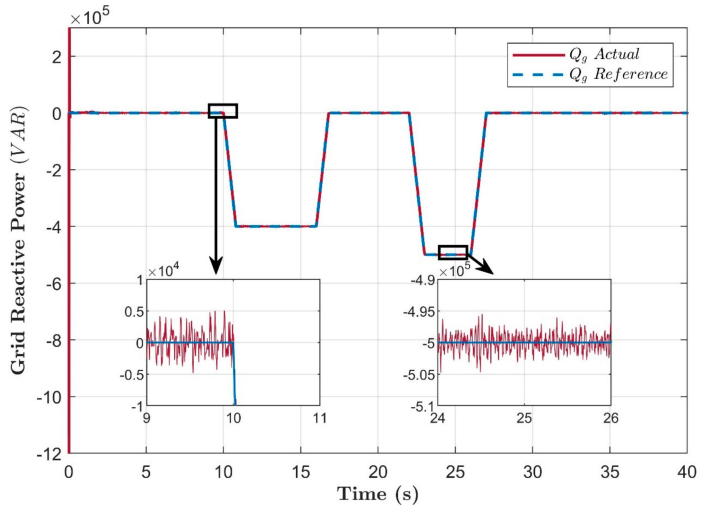

Figure 27. DFIG grid side reactive power variation.

The quadrature and direct current components are responsible for the independent control over active and reactive power flow. Figure 28 presents the reference tracking of the quadrature component of the rotor current. Figure 29 shows the quadrature current and direct current component of the grid current. The yellow line shows the reference quadrature grid current and the red line presents the actual quadrature grid current. The purple line shows the reference direct grid current and the green line presents the actual direct grid current. During the simulation references for the direct and quadrature grid current are changed. The proposed controllers show good tracking under reference variation.

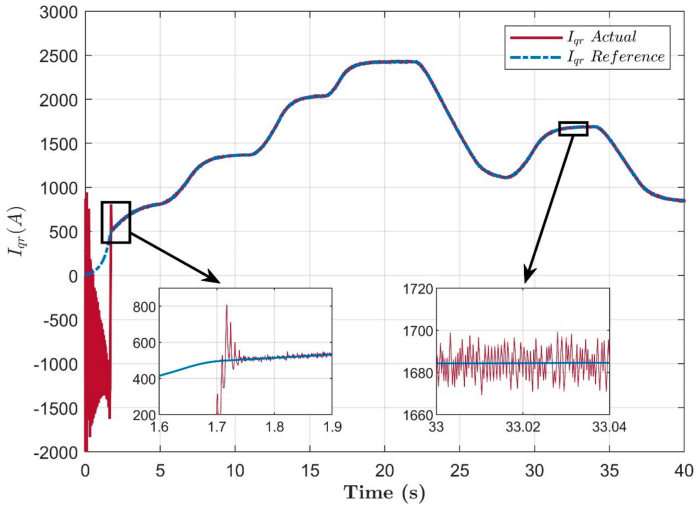

Figure 28. Reference and actual quadrature rotor current tracking performance.

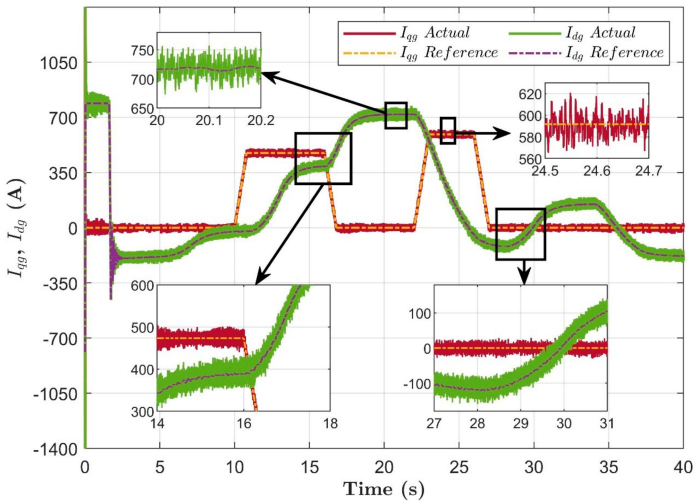

Figure 29. Tracking performance of direct and quadrature current component of GSC.

The reference voltage for the DC link is set to the value of 1150 V. The actual DC link voltage follows the reference very well without the overshooting, and deviation from the reference value is only about 1 V even if the wind speed is changed as is shown in Figure 30. The power flow in the DC link is bidirectional.

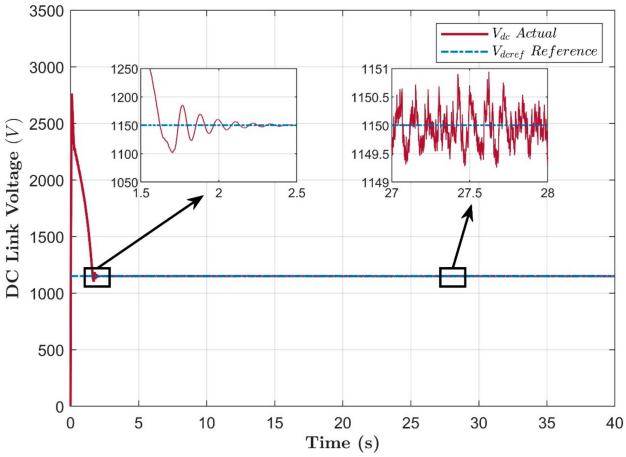

Figure 30. Tracking performance of DC link voltage.

The THD analysis for the stator current from the frequency range of 0 Hz to 1 kHz for three cycles with the fundamental frequency of 50 Hz is shown in Figure 31. This clearly shows that when the generator runs at its rated speed, the THD content in the stator current is only 0.73%.

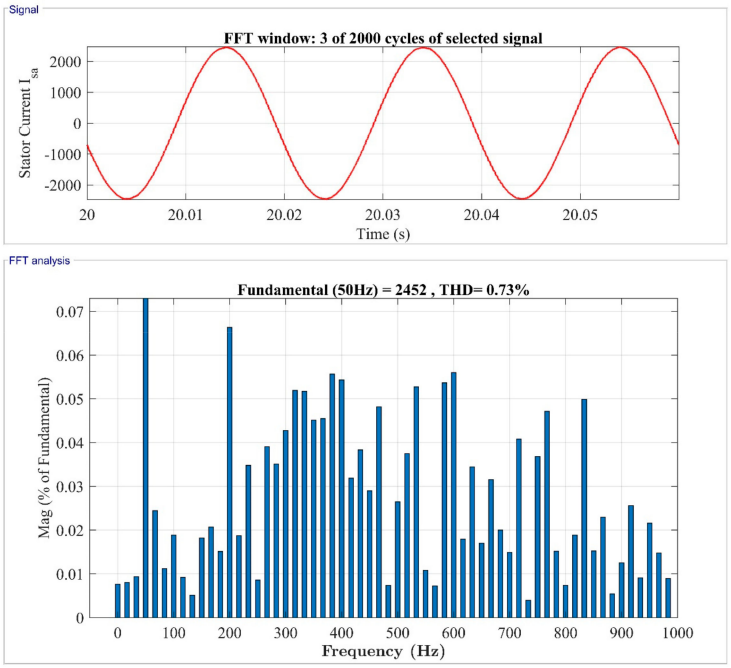

Figure 31. THD performance of single-phase stator current.

Figure 32 shows the THD analysis for the grid current for three cycles, with a frequency range of 0 Hz to 1 kHz with the fundamental frequency of 50 Hz. As seen from Figure 32, the THD content in grid current is only 3.86%, according to IEEE standards.

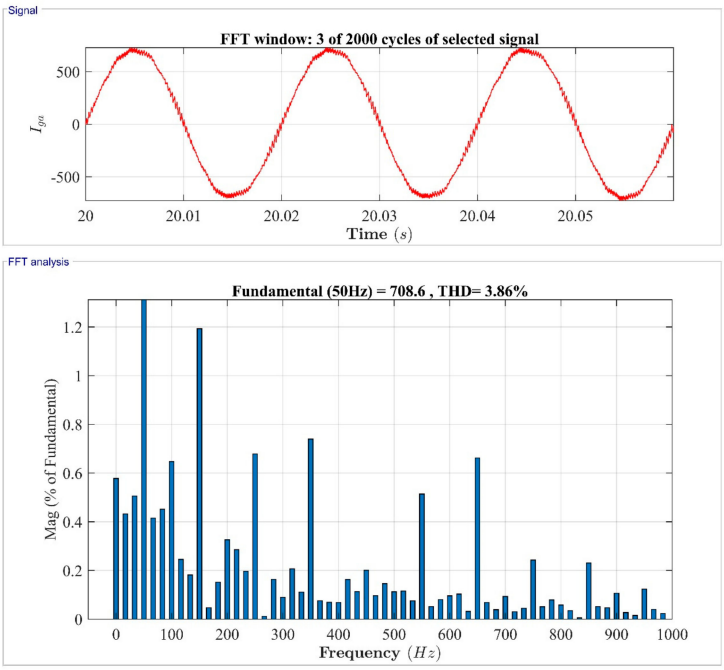

Figure 32. THD performance of single-phase grid current.

From the simulation analysis and all the figures, we conclude that MPPT control shows good power tracking performance under different wind speed conditions. The vector control strategy for RSC and GSC with PI regulators shows good dynamic performance and reference tracking without overshooting. The proposed controls ensure good dynamic and transient performance with maximum power extraction from the wind.

7. Conclusions

The modeling and control of grid-connected DFIG-based WECS has been proposed in this study. At first, the mathematical model of turbine and DFIG are proposed. The proposed MPPT controller works efficiently with wind speed variation and tracks the power very well, even in low wind conditions to the wide wind speed variation. The vector control strategy for the RSC and GSC have been proposed for the power flow control between the grid and the DFIG system. The stator voltage and current waveform are balanced and sinusoidal. The simulation study shows that the proposed system with a control strategy works satisfactorily and gives good performance under wind speed variation. THD analysis shows that the stator current and grid current THD is according to IEEE 519 standard. Moreover, results show fast response time, no overshoot, and robustness of the proposed system. This research may be further explored, considering the variable pitch angle along with multi-input variables. Performance may also be contrasted with other controller types based on artificial intelligence, model reference adaptive system that may be substituted in the RSC and GSC schemes.

Author Contributions: Conceptualization, A.A.C., P.C. and A.N.V.; methodology, P.C. and V.B.; investigation, A.A.C., T.C. and S.G.; formal analysis, V.B., G.S. and A.N.V.; validation, V.B., G.S. and A.K.; resources and data curation, A.A.C. and V.B.; writing—original draft preparation, A.A.C., T.C. and S.G.; writing review and editing, P.C. and V.B.; visualization, A.A.C., V.B. and TC.; supervision, P.C., V.B. and G.S.; project administration, P.C.; funding acquisition, V.B., G.S., A.N.V. and A.K. All authors have read and agreed to the published version of the manuscript.

Funding: This research received no external funding.

Informed Consent Statement: Not applicable.

Data Availability Statement: Data are available on request to abrar0613@gmail.com.

Conflicts of Interest: The authors declare no conflict of interest.

References

1. Chhipa, A.A.; Kumar, V.; Vyas, S.; Joshi, R.R. MPPT Optimisation Techniques and Power Electronics for Renewable Energy Systems: Wind and Solar Energy Systems. *Int. J. Swarm Intell.* **2021**, *1*, 1. [CrossRef]
2. Qazi, A.; Hussain, F.; Rahim, N.A.B.D.; Hardaker, G.; Alghazzawi, D.; Shaban, K.; Haruna, K. Towards Sustainable Energy: A Systematic Review of Renewable Energy Sources, Technologies, and Public Opinions. *IEEE Access* **2019**, *7*, 63837–63851. [CrossRef]
3. Prasad, R.M.; Mulla, M.A. Mathematical Modeling and Position-Sensorless Algorithm for Stator-Side Field-Oriented Control of Rotor-Tied DFIG in Rotor Flux Reference Frame. *IEEE Trans. Energy Convers.* **2020**, *35*, 631–639. [CrossRef]
4. Hu, J.; Nian, H.; Xu, H.; He, Y. Dynamic Modeling and Improved Control of DFIG under Distorted Grid Voltage Conditions. *IEEE Trans. Energy Convers.* **2011**, *26*, 163–175. [CrossRef]
5. Hosseini, S.H.; Sharifian, M.B.B.; Shahnia, F. Dynamic Performance of Double Fed Induction Generator for Wind Turbines. In Proceedings of the ICEMS 2005 Eighth International Conference on Electrical Machines and Systems, Nanjing, China, 27–29 September 2005; Volume 2, pp. 1261–1266. [CrossRef]
6. Balat, M.; Balat, H. Biogas as a Renewable Energy Sourcea Review. *Energy Sources Part A Recovery Util. Environ. Eff.* **2009**, *31*, 1280–1293. [CrossRef]
7. Chhipa, A.A.; Vyas, S.; Kumar, V.; Joshi, R.R. Role of Power Electronics and Optimization Techniques in Renewable Energy Systems. In *Intelligent Algorithms for Analysis and Control of Dynamical Systems. Algorithms for Intelligent Systems*; Springer: Singapore, 2021; pp. 167–175. [CrossRef]
8. Hansen, A.D.; Sørensen, P.; Lov, F.; Blaabjerg, F. Control of Variable Speed Wind Turbines with Doubly-Fed Induction Generators. *Wind Eng.* **2004**, *28*, 411–432. [CrossRef]
9. Tanvir, A.A.; Merabet, A.; Beguenane, R. Real-Time Control of Active and Reactive Power for Doubly Fed Induction Generator (DFIG)-Based Wind Energy Conversion System. *Energies* **2015**, *8*, 10389–10408. [CrossRef]

10. Poitiers, F.; Bouaouiche, T.; Machmoum, M. Advanced Control of a Doubly-Fed Induction Generator for Wind Energy Conversion. *Electr. Power Syst. Res.* **2009**, *79*, 1085–1096. [CrossRef]
11. Rezaei, E.; Tabesh, A.; Ebrahimi, M. Dynamic Model and Control of DFIG Wind Energy Systems Based on Power Transfer Matrix. *IEEE Trans. Power Deliv.* **2012**, *27*, 1485–1493. [CrossRef]
12. Zou, Y.; Elbuluk, M.; Sozer, Y. A Complete Modeling and Simulation of Induction Generator Wind Power Systems. In Proceedings of the Conference Record-IAS Annual Meeting (IEEE Industry Applications Society), Houston, TX, USA, 3–7 October 2010. [CrossRef]
13. Idrissi, I.; Chafouk, H.; El Bachtiri, R.; Khanfara, M. Modeling and Simulation of the Variable Speed Wind Turbine Based on a Doubly Fed Induction Generator. In *Gas Turbines-Control, Diagnostics, Simulation, and Measurements*; IntechOpen: London, UK, 2019. [CrossRef]
14. Ullah, N.R.; Thiringer, T. Variable Speed Wind Turbines for Power System Stability Enhancement. *IEEE Trans. Energy Convers.* **2007**, *22*, 52–60. [CrossRef]
15. Chhipa, A.A.; Kumar, V.; Joshi, R.R.; Chakrabarti, P.; Jasinski, M.; Burgio, A.; Leonowicz, Z.; Jasinska, E.; Soni, R.; Chakrabarti, T. Adaptive Neuro-Fuzzy Inference System-Based Maximum Power Tracking Controller for Variable Speed WECS. *Energies* **2021**, *14*, 6275. [CrossRef]
16. Rao, K.R. Wind Energy: Technical Considerations–Contents. In *Wind Energy for Power Generation*; Springer: Cham, Switzerland, 2019; pp. 1–426. [CrossRef]
17. Xiahou, K.; Liu, Y.; Wang, L.; Li, M.S.; Wu, Q.H. Control of DFIG's Rotor-Side Converter with Decoupling of Current Loops Using Observer-Based Fractional-Order Sliding-Mode Regulators. *IEEE Access* **2019**, *7*, 163412–163420. [CrossRef]
18. Yao, J.; Li, H.; Chen, Z.; Xia, X.; Chen, X.; Li, Q.; Liao, Y. Enhanced Control of a DFIG-Based Wind-Power Generation System with Series Grid-Side Converter under Unbalanced Grid Voltage Conditions. *IEEE Trans. Power Electron.* **2013**, *28*, 3167–3181. [CrossRef]
19. Rajendran, M.; Kumar, L.A. Modeling and Simulation of a Dfig-Based Wind Energy System. In *Lecture Notes in Electrical Engineering*; Springer: Singapore, 2020; Volume 687, pp. 31–49. [CrossRef]
20. Nian, H.; Xu, Y.; Chen, L.; Zhu, M. Modeling and Analysis of DC-Link Dynamics in DFIG System with an Indicator Function. *IEEE Access* **2019**, *7*, 125401–125412. [CrossRef]
21. Karabacak, K.; Cetin, N. Artificial Neural Networks for Controlling Wind-PV Power Systems: A Review. *Renew. Sustain. Energy Rev.* **2014**, *29*, 804–827. [CrossRef]
22. Marugán, A.P.; Márquez, F.P.G.; Perez, J.M.P.; Ruiz-Hernández, D. A Survey of Artificial Neural Network in Wind Energy Systems. *Appl. Energy* **2018**, *228*, 1822–1836. [CrossRef]
23. Gayatri, M.T.L.; Parimi, A.M.; Pavan Kumar, A.V. A Review of Reactive Power Compensation Techniques in Microgrids. *Renew. Sustain. Energy Rev.* **2018**, *81*, 1030–1036. [CrossRef]
24. Geng, H.; Liu, C.; Yang, G. LVRT Capability of DFIG-Based WECS under Asymmetrical Grid Fault Condition. *IEEE Trans. Ind. Electron.* **2013**, *60*, 2495–2509. [CrossRef]
25. Singh, G.K. Self-Excited Induction Generator Research—A Survey. *Electr. Power Syst. Res.* **2004**, *69*, 107–114. [CrossRef]
26. Singh, B.; Murthy, S.S.; Gupta, S. A Voltage and Frequency Controller for Self-Excited Induction Generators. *Electr. Power Compon. Syst.* **2006**, *34*, 141–157. [CrossRef]
27. McPherson, G. Analysis of the Isolated Induction Generator. *IEEE Trans. Power Appar. Syst.* **1983**, *8*, 2793–2798. [CrossRef]
28. Casielles, P.G.; Sanz, J.; Pascual, J. Control System for a Wind Turbine Driven Self Excited Asynchronous Generator. In Proceedings of the Electrotechnical Conference Integrating Research, Industry and Education in Energy and Communication Engineering, Lisbon, Portugal, 11–13 April 1989; pp. 95–98. [CrossRef]
29. Kasal, G.K.; Singh, B. Voltage and Frequency Controllers for an Asynchronous Generator-Based Isolated Wind Energy Conversion System. *IEEE Trans. Energy Convers.* **2011**, *26*, 402–416. [CrossRef]
30. Peña, R.; Cárdenas, R.; Escobar, E.; Clare, J.; Wheeler, P. Control System for Unbalanced Operation of Stand-Alone Doubly Fed Induction Generators. *IEEE Trans. Energy Convers.* **2007**, *22*, 544–545. [CrossRef]
31. Jain, A.K.; Ranganathan, V.T. Wound Rotor Induction Generator with Sensorless Control and Integrated Active Filter for Feeding Nonlinear Loads in a Stand-Alone Grid. *IEEE Trans. Ind. Electron.* **2008**, *55*, 218–228. [CrossRef]
32. Goel, P.K.; Singh, B.; Murthy, S.S.; Kishore, N. Parallel Operation of DFIGs in Three-Phase Four-Wire Autonomous Wind Energy Conversion System. *IEEE Trans. Ind. Appl.* **2011**, *47*, 1872–1883. [CrossRef]
33. Watson, D.B.; Arrillaga, J.; Densem, T. Controllable d.c. power supply from wind-driven self-excited induction machines. *Proc. Inst. Electr. Eng.* **1979**, *126*, 1245–1248. [CrossRef]
34. Chen, W.; Liming, W.; Libao, S.; Yixin, N. A Survey on Wind Power Technologies in Power Systems. In Proceedings of the 2007 IEEE Power Engineering Society General Meeting, PES, Tampa, FL, USA, 24–28 June 2007. [CrossRef]
35. Hinrichsen, E.N. Controls for Variable Pitch Wind Turbine Generators. *IEEE Trans. Power Appar. Syst.* **1984**, *4*, 886–892. [CrossRef]
36. Yamamoto, M.; Motoyoshi, O. Active and Reactive Power Control for Doubly-Fed Wound Rotor Induction Generator. *IEEE Trans. Power Electron.* **1991**, *6*, 624–629. [CrossRef]
37. Uctug, M.Y.; Eskandarzadeh, I.; Ince, H. Modelling and Output Power Optimisation of a Wind Turbine Driven Double Output Induction Generator. *IEE Proc. Electr. Power Appl.* **1994**, *141*, 33–38. [CrossRef]

38. Arnaltes Gómez, S.; Rodriguez Amenedo, J.L. Grid Synchronisation of Doubly Fed Induction Generators Using Direct Torque Control. In Proceedings of the IEEE 2002 28th Annual Conference of the Industrial Electronics Society. IECON, Seville, Spain, 5–8 November 2002; Volume 4, pp. 3338–3343. [CrossRef]
39. Tapia, A.; Tapia, G.; Xabier Ostolaza, J.; Sáenz, J.R. Modeling and Control of a Wind Turbine Driven Doubly Fed Induction Generator. *IEEE Trans. Energy Convers.* **2003**, *18*, 194–204. [CrossRef]
40. Jabr, H.M.; Kar, N.C. Adaptive Vector Control for Slip Energy Recovery in Doubly-Fed Wind Driven Induction Generator. In Proceedings of the Canadian Conference on Electrical and Computer Engineering, Saskatoon, SK, Canada, 1–4 May 2005; Volume 2005, pp. 759–762. [CrossRef]
41. Jiao, L.; Ooi, B.T.; Joós, G.; Zhou, F. Doubly-Fed Induction Generator (DFIG) as a Hybrid of Asynchronous and Synchronous Machines. *Electr. Power Syst. Res.* **2005**, *76*, 33–37. [CrossRef]
42. Tremblay, E.; Chandra, A.; Lagacé, P.J. Grid-Side Converter Control of DFIG Wind Turbines to Enhance Power Quality of Distribution Network. In Proceedings of the 2006 IEEE Power Engineering Society General Meeting, PES, Montreal, QC, Canada, 18–22 June 2006. [CrossRef]
43. Chowdhury, B.H.; Chellapilla, S. Double-Fed Induction Generator Control for Variable Speed Wind Power Generation. *Electr. Power Syst. Res.* **2006**, *76*, 786–800. [CrossRef]
44. Datta, R.; Ranganathan, V.T. Decoupled Control of Active and Reactive Power for a Grid-Connected Doubly-Fed Wound Rotor Induction Machine without Position Sensors. In Proceedings of the Conference Record-IAS Annual Meeting (IEEE Industry Applications Society), Phoenix, AZ, USA, 3–7 October 1999; Volume 4, pp. 2623–2630. [CrossRef]
45. Datta, R.; Ranganathan, V.T. Direct Power Control of Grid-Connected Wound Rotor Induction Machine without Rotor Position Sensors. *IEEE Trans. Power Electron.* **2001**, *16*, 390–399. [CrossRef]
46. Ying, L.M.; Cui, X.; Liao, Q.F.; Tang, C.H.; Le, L.C.; Chen, Z. Stator Flux Observation and Speed Estimation of a Doubly Fed Induction Generator. In Proceedings of the 2006 International Conference on Power System Technology, POWERCON2006, Chongqing, China, 22–26 October 2006. [CrossRef]
47. Qiao, W.; Zhou, W.; Aller, J.M.; Harley, R.G. Wind Speed Estimation Based Sensorless Output Maximization Control for a Wind Turbine Driving a DFIG. *IEEE Trans. Power Electron.* **2008**, *23*, 1156–1169. [CrossRef]
48. Hongfei, M.; Yi, W.; Dianguo, X.; Yongqiang, L. Research on AC-DC-AC Converter for Wind Power Doubly-Fed Induction Generator. In Proceedings of the IECON Proceedings (Industrial Electronics Conference), Paris, France, 6–10 November 2006; pp. 2734–2739. [CrossRef]
49. Pena, R.S.; Cardenas, R.J.; Asher, G.M.; Clare, J.C. Vector Controlled Induction Machines for Stand-Alone Wind Energy Applications. In Proceedings of the Conference Record of the 2000 IEEE Industry Applications Conference. Thirty-Fifth IAS Annual Meeting and World Conference on Industrial Applications of Electrical Energy, Rome, Italy, 8–12 October 2000; Volume 3, pp. 1409–1415. [CrossRef]
50. Cárdenas, R.; Peña, R.; Proboste, J.; Asher, G.; Clare, J. MRAS Observer for Sensorless Control of Standalone Doubly Fed Induction Generators. *IEEE Trans. Energy Convers.* **2005**, *20*, 710–718. [CrossRef]
51. Hilloowala, R.M.; Sharaf, A.M. A Rule-Based Fuzzy Logic Controller for a PWM Inverter in a Stand Alone Wind Energy Conversion Scheme. *IEEE Trans. Ind. Appl.* **1996**, *32*, 57–65. [CrossRef]
52. Simões, M.G.; Bose, B.K.; Spiegel, R.J. Design and Performance Evaluation of a Fuzzy-Logic-Based Variable-Speed Wind Generation System. *IEEE Trans. Ind. Appl.* **1997**, *33*, 956–965. [CrossRef]
53. Poddar, G.; Joseph, A.; Unnikrishnan, A.K. Sensorless Variable-Speed Controller for Existing Fixed-Speed Wind Power Generator with Unity-Power-Factor Operation. *IEEE Trans. Ind. Electron.* **2003**, *50*, 1007–1015. [CrossRef]
54. Teodorescu, R.; Blaabjerg, F. Flexible Control of Small Wind Turbines with Grid Failure Detection Operating in Stand-Alone and Grid-Connected Mode. *IEEE Trans. Power Electron.* **2004**, *19*, 1323–1332. [CrossRef]
55. Ahmed, T.; Nishida, K.; Nakaoka, M. Advanced Control of PWM Converter with Variable-Speed Induction Generator. *IEEE Trans. Ind. Appl.* **2006**, *42*, 934–945. [CrossRef]
56. Ahmed, T.; Nishida, K.; Nakaoka, M. Advanced Control for PWM Converter and Variable-Speed Induction Generator. *IET Electr. Power Appl.* **2007**, *1*, 239–247. [CrossRef]
57. Barakati, S.M.; Kazerani, M.; Aplevich, J.D. Maximum Power Tracking Control for a Wind Turbine System Including a Matrix Converter. *IEEE Trans. Energy Convers.* **2009**, *24*, 705–713. [CrossRef]
58. Kazmi, S.M.R.; Goto, H.; Guo, H.J.; Ichinokura, O. A Novel Algorithm for Fast and Efficient Speed-Sensorless Maximum Power Point Tracking in Wind Energy Conversion Systems. *IEEE Trans. Ind. Electron.* **2011**, *58*, 29–36. [CrossRef]
59. Vas, P.; Li, J. Simulation package for vector controlled induction motor drives. In Proceedings of the 1993 Sixth International Conference on Electrical Machines and Drives, Oxford, UK, 8–10 September 1993; pp. 265–270. Available online: https://ieeexplore.ieee.org/document/253528 (accessed on 3 September 2022).
60. Gabriel, R.; Leonhard, W.; Nordby, C.J. Field-Oriented Control of a Standard AC Motor Using Microprocessors. *IEEE Trans. Ind. Appl.* **1980**, *2*, 186–192. [CrossRef]
61. Wu, Y.K.; Yang, W.H. Different Control Strategies on the Rotor Side Converter in DFIG-Based Wind Turbines. *Energy Procedia* **2016**, *100*, 551–555. [CrossRef]
62. Hore, D.; Sarma, R. Neural Network–based Improved Active and Reactive Power Control of Wind-Driven Double Fed Induction Generator under Varying Operating Conditions. *Wind Eng.* **2018**, *42*, 381–396. [CrossRef]

63. Carroll, J.; McDonald, A.; McMillan, D. Reliability Comparison of Wind Turbines with DFIG and PMG Drive Trains. *IEEE Trans. Energy Convers.* **2015**, *30*, 663–670. [CrossRef]
64. Hosseini, S.M.H.; Rezvani, A. Modeling and Simulation to Optimize Direct Power Control of DFIG in Variable-Speed Pumped-Storage Power Plant Using Teaching–learning-Based Optimization Technique. *Soft Comput.* **2020**, *24*, 16895–16915. [CrossRef]
65. Xia, Y.; Chen, Y.; Song, Y.; Strunz, K. Multi-Scale Modeling and Simulation of DFIG-Based Wind Energy Conversion System. *IEEE Trans. Energy Convers.* **2020**, *35*, 560–572. [CrossRef]
66. Abad, G.; López, J.; Rodríguez, M.A.; Marroyo, L.; Iwanski, G. *Doubly Fed Induction Machine: Modeling and Control for Wind Energy Generation*; Institute of Electrical and Electronics Engineers: Piscataway, NJ, USA, 2011. [CrossRef]